Optik - International Journal for Light and Electron Optics xxx (xxxx) xxxx

Contents lists available at ScienceDirect

Optik

journal homepage: www.elsevier.com/locate/ijleo

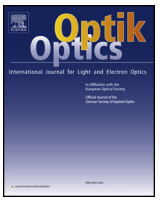

Original research article

Transmissivity assessment of plasmonic-dielectric waveguide interconnects via modified FFT-BPM

Adel Shaaban[a,b], Yi-Chun Du[a,*], Lotfy Rabeh Gomaa[c]

[a] Department of Electrical Engineering, Southern Taiwan University of Science and Technology, Tainan 71005, Taiwan
[b] Department of Radiation Engineering, National Center for Radiation Research (NCRRT), Atomic Energy Authority, Cairo 11765, Egypt
[c] Faculty of Engineering at Shobra, Banha University, Cairo 11672, Egypt

ARTICLE INFO

Keywords:
FFT-based beam propagation method (FFT-BPM)
Transverse magnetic (TM)
Finite-difference frequency-domain (FDFD)
Biosensors

ABSTRACT

We present remedies to two fundamental difficulties facing the applicability of the traditional FFT-based beam propagation method (FFT-BPM) when investigating the propagation and transmission of transverse magnetic (TM) optical beams in subwavelength step-index waveguiding structures. To the best of our knowledge, the FFT-BPM is introduced for the first time to assess the plasmonic-dielectric waveguide interconnects. At the junction plane, we modified the FFT-BPM algorithm by including a combined spatial-spectral reflection operator formalism to calculate the reflected field. As a test, we calculated the optical power transmission efficiency between plasmonic and dielectric waveguide interconnect. A comparison between our results, and those obtained by full-modal matching using finite-difference frequency-domain (FDFD), reveals good agreement. Such interconnecting structure is crucial in many applications as biosensors, optical near-field probes, and interfacing elements involving high-contrast refractive index materials. We believe that rehabilitating the classical FFT-BPM to handle nanoscale waveguiding structures, which include metal-dielectric interfaces, will be of prime importance in the development, analysis and assessment of nano-photonics devices.

1. Introduction

The increasing demand for fast information transport and processing is undeniable. This has driven enormous progress in the silicon electronics technology. The last few decades have witnessed a huge progression towards faster, smaller and more efficient electronic devices. The scaling of these sophisticated devices has brought about many challenges. Perhaps, the most daunting problems preventing significant increase in processor speed are thermal and signal propagation delay issues associated with electronic interconnections. On the other hand, optical interconnects, have an extremely large data, carrying capacity, that may offer new promising solutions to circumvent these problems. Optical alternatives are particularly attractive for next generation chips in which a multitude of fast electronic processors need to be connected by high-speed interconnectors. Unfortunately, the large size mismatch between electronic and dielectric photonic devices hampers the implementation of such processors. As the dielectric photonic devices are diffraction-limited in size to about half the light wavelength, so that they are at least one or two orders of magnitude larger than their nanoscale electronic counterparts. This size mismatch presents a major challenge when interfacing these technologies. For further progress, it is required a substantially new chip-scale device technology [1] that can facilitate information transmission between nano-scale devices at optical frequencies and hence bridge the gap between micro-scale photonics and nano-scale

* Corresponding author.
E-mail address: terrydu@stust.edu.tw (Y.-C. Du).

https://doi.org/10.1016/j.ijleo.2019.164143
Received 27 November 2019; Accepted 27 December 2019

electronics.

Fortunately, surface plasmon-based interconnect structures can merge electronics and photonics at nanoscale [2], and thus offer a reliable solution to that size-compatibility problem. The most remarkable feature of subwavelength metallic waveguiding structures is their high degree of concentration of electromagnetic fields achievable in the vicinity of metal surfaces. This degree of concentration, which is well beyond the diffraction limit, arises from coupling the energy and momentum of a photon to a free-electron gas in the metal. The subwavelength coupled oscillations, known as surface plasmons (SPs), both enable efficient light manipulation at the nanoscale in plasmonic structures. Few years ago [3], an insulator-metal-insulator (IMI) plasmonic interconnect using TiN has been proposed and investigated experimentally at wavelength 1.55 μm. This enables the developers and chip designers to implement minute electronic circuits that can move data very fast across the chip. In this respect, plasmonic devices could be considered as one of the most promising candidates able to overcome the size mismatch between microscale photonic devices and nanoscale electronics [4–7]. It is worthy to note that, due to remarkable field confinement near the interface and around sharp corners [8], surface plasmons are very well suited for bio-sensors [9], near field imaging [10–12] and storage devices [13]. Also, the distinct enhancement of light emission when InGaN/GaN quantum wells are coated by nanometer silver films, renders the surface plasmons an exceptional promoter for the internal quantum efficiency in optical sources [14].

The theoretical analysis and assessment of such subwavelength metallic waveguiding structures represent a heavy computational load that should be handled efficiently. The finite difference time domain (FDTD) and the finite difference frequency domain (FDFD) are the most widely used numerical methods for plasmonic simulation and analysis [15]. Surprisingly, to the best of our knowledge, the FFT-based beam propagation method (FFT-BPM) has not been used, so far, to study and investigate the propagation and coupling of optical beams in sub-wavelength plasmonic-dielectric waveguides interconnects.

Declining the use of FFT-BPM in such problems, motivated us to reconsider the major difficulties associated with TM fields [16] in the framework of the BPM. Two major reasons behind this declination are: firstly, the mixing of field derivative and refractive index derivative in the wave equation; secondly, the step-like discontinuity in the refractive index profile of both: dielectric and plasmonic waveguide as well [17]. In this paper, we present two possible remedies for these difficulties. It is worthy to note that these remedies are not merely a way to improve the accuracy, but rather they are indispensable to adapt the traditional FFT-BPM to handle TM fields. This allows getting full benefit of the simplicity and powerfulness of the FFT-based BPM. Obviously, on one hand, the presence of mixed derivatives of the field and the refractive index profile in the wave equation of the TM field prevents the direct use of FFT in the BPM algorithm for such type of fields. On the other hand, the equivalent index required to transform the TM problem to an equivalent TE, involves transverse second derivative of the discontinuous step-index at the interface metal-dielectric forming the boundaries of the plasmonic waveguide. That is, a Dirac-delta singularity will occur in the derivative unless a suitable smoothing approximation to the step-index profile is applied.

It is worthy to note that, spectral domain methods (like FFT-BPM) are more superior than spatial domain-based methods (Finite difference (FD) and Finite element (FE)) especially when considering subwavelength structures [18]. This is why most of the FD-based methods are performed in the spectral domain (FDFD) when considering nanoscale structures [19,20]. Though, FD schemes are usually stable numerically, they may not conserve power even when used in conjunction with vectorial beam propagation methods [21]. To make our exposition clear, we shall consider two-dimensional waveguiding structures with the optical power confined in one dimension.

2. Reconsideration of TM fields difficulties

Fig. 1, depicts a one-dimensional (y-invariant) metal-insulator-metal (MIM) plasmonic waveguide. The modes of such guide are TM in nature with the magnetic field H_y and the electric fields E_x and E_z derivable from the magnetic field H_y [22]. The refractive index of the metal n_m is complex:

$$n_m = n_{mr} - jn_{mi} \tag{1}$$

where, n_{mr} and n_{mi} are the real and imaginary parts respectively. Assuming a monochromatic time-harmonic dependence of the form $e^{j\omega t}$ (j being the imaginary unit and ω is the angular frequency), the wave equation for $H_y(x,z)$ takes the form [17]:

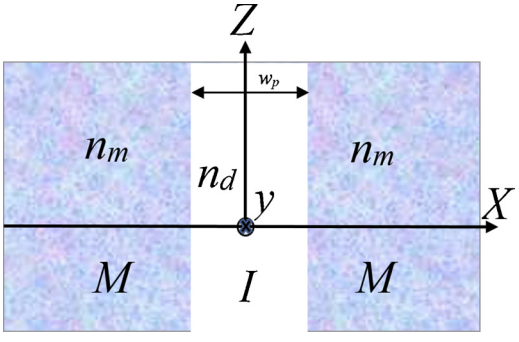

Fig. 1. Schematic diagram of a 2-dimmensional MIM plasmonic waveguide.

$$\left[\nabla^2 + k_0^2 n_p^2(x) - \frac{1}{n_p^2(x)}\frac{\partial n_p^2(x)}{\partial x}\frac{\partial}{\partial x}\right] H_y(x, z) = 0 \tag{2}$$

where k_o is the free space wavenumber, $\nabla^2 = (\partial^2/\partial x^2 + \partial^2/\partial z^2)$ and $n_p(x)$ is the refractive index profile of the plasmonic waveguide composed of a dielectric layer with refractive index n_d surrounded by a metal with index n_m. The dielectric could be lossy, but for the moment, we shall assume it lossless. As stated earlier, the first problem facing the applicability of the FFT-based BPM in the solution of Eq. (2) is the term involving the mixed derivatives of the field and the refractive index profile. Poladian et al. [17] suggested a transformation of the TM problem to a TE one via the following transformation:

$$H_y(x, z) = n_p(x)F(x, z) \tag{3}$$

direct substitution of Eq. (3) in Eq. (2) results in the following wave equation for F(x,z):

$$\nabla^2 F + k_o^2[n_p^2(x) - \frac{n_p(x)}{k_o^2}\frac{\partial^2}{\partial x^2}(\frac{1}{n^p(x)})]F = 0 \tag{4}$$

this can be written as:

$$[\nabla^2 + k_o^2 n_{eq}^2(x)]F = 0 \tag{5}$$

It is easy to conclude that Eq. (5) is a TE problem with an equivalent index medium:

$$n_{eq}^2(x) = n_p^2(x) - \frac{n_p(x)}{k_o^2}\frac{\partial^2}{\partial x^2}(\frac{1}{n^p(x)}) \tag{6}$$

The equivalent problem Eq. (5) is amenable -in principle- to be solved via the traditional FFT-based BPM algorithm. However, the step-like index profile $n_p(x)$ represents the second major problem that should be treated carefully. A judicious solution is to approximate $n_p(x)$ by a "smooth" function in order to circumvent the singularity in the transverse derivative $\partial_x^2(1/n^p(x))$ in the equivalent index Eq. (6).

Some authors [22,23] suggested to use a sigmoid smoothing function in the analysis of TM modes of planar lossless dielectric waveguides. But, they pointed out that the choice of the smoothing parameter in the sigmoid function is very sensitive in concern with power conservation, and can introduce spurious modes if its value is not well chosen [22]. Other authors [24] used an arctangent function as a smoothing function, but sometimes, numerical artifacts may appear on the sharp boundaries of the guiding structure if the steepness parameter is not chosen cautiously [22]. In this paper, we adopted the smooth transition autoregressive (STAR) function [25] to approximate the refractive step-index profile $n_p(x)$ of the MIM plasmonic guide. This function did not suffer from the previously mentioned drawbacks, especially when calculating the second derivative of the inverse of the refractive index profile numerically (c.f. Eq. 6). Accordingly, the STAR function assumes the following form:

$$n_{pa}(x) = n_m + \frac{n_m e^{-(aW_p/2)} + n_d e^{ax}}{e^{-(aW_p/2)} + e^{ax}} - \frac{n_m e^{(aW_p/2)} + n_d e^{ax}}{e^{(aW_p/2)} + e^{ax}} \tag{7}$$

where, 'a', is a parameter (its unit is the inverse of x) which describes the steepness of the function n_{pa}. Fig. 2, depicts the smooth profile n_{pa} for different values of 'a'. The width of the guide is $W_p = 50$ nm, the metal is silver having $n_m = 0.397$ - j11.4 at $\lambda = 1.55$ μm [19], and the dielectric core is air ($n_d = 1$). From the numerical perspective, we found that when 'a' lies in the range 5–40, $n_{pa}(x)$ gives a satisfactory approximation to the original step-index profile $n_p(x)$, as shown in Fig. 2.

3. The dielectric-plasmonic Butt-Coupler

Fig. 3 shows a dielectric waveguide with width $W_d = 300$ nm, butt-coupled to a plasmonic MIM waveguide having a width W_p. The width 300 nm of the dielectric guide corresponds to the minimum spot size of the fundamental TM_0 mode at $\lambda_o = 1.55$ μm. While

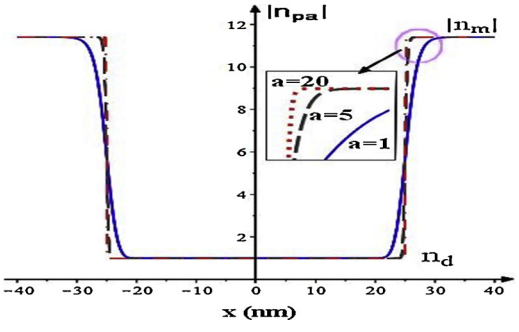

Fig. 2. Smoothing function $n_{pa}(x)$ for different values of the steepness parameter 'a'.
Obviously, Eq. (7) could be applied to step-index dielectric waveguides as well.

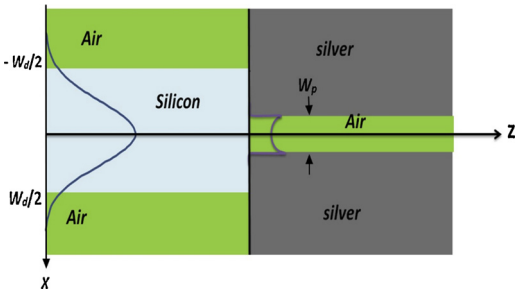

Fig. 3. Butt-coupling between dielectric waveguide and MIM waveguide. The TM_0 mode of the dielectric guide is incident on the z = 0 plane, where the fundamental TM_0 mode of the plasmonic guide is excited as well as the continuous spectrum.

the width of the plasmonic guide W_p is varied in the range 5–200 nm. Upon the incidence of the TM_0 mode from the dielectric guide on the interface plane z = 0, backward reflected and forwarded transmitted fields are generated. The calculation of the reflected field is carried out using a combined spatial-spectral formalism [26]. This enables us to express the reflected field $H_r(x,z)$ at the junction plane z = 0 as follows:

$$H_r(x, 0) = \Delta r(x, 0) \cdot \mathcal{F}^{-1}[h_i(k_x, 0) \cdot \rho(k_x, 0)] \tag{8}$$

where $h_i(k_x,0)$ is the angular spectrum representation, i.e. the transverse Fourier transform (with respect to x) of the incident field $H_i(x,0)$ at the junction plane (the fundamental guided mode TM_0 of the dielectric waveguide). This plane wave spectrum takes the form [27,28]:

$$h_i(k_x, 0) = \int_{-\infty}^{\infty} H_i(x, 0) e^{-jk_x x} dx \tag{9}$$

where, k_x is the variable of the Fourier transform. The spectral part $\rho(k_x,0)$ of the reflection formalism in the inverse Fourier transform $\mathfrak{F}^{-1}$ in Eq. (8), is the Fresnel reflection coefficient corresponding to the plane wave component $h_i(k_x,0)$. It assumes the form [26]:

$$\rho(k_x, 0) = \frac{k_z^- \cdot (n_o^+)^2 - k_z^+ \cdot (n_o^-)^2}{k_z^- \cdot (n_o^+)^2 + k_z^+ \cdot (n_o^-)^2} \tag{10}$$

where, n_o^+ and n_o^- are certain reference refractive indices just immediately after and before the junction plane z = 0 as will be explained later. k_z^+ and k_z^- are the z-components of wave vectors of the angular spectrum of plane waves having transverse x-components k_x in the regions z > 0 and z < 0 respectively. Namely, they are written as [26]:

$$k_z^- = \sqrt{k_o^2 (n_0^-)^2 - k_x^2} \tag{11}$$

$$k_z^+ = \sqrt{k_o^2 (n_0^+)^2 - k_x^2} \tag{12}$$

the spatial dependent part of the reflection $\Delta r(x, 0)$ in Eq. (8) takes the form [26]:

$$\Delta r(x, 0) = \frac{r(x, 0)}{r_0} \tag{13}$$

where:

$$r(x, 0) = \frac{n(x, 0^+) - n(x, 0^-)}{n(x, 0^+) + n(x, 0^-)} \tag{14}$$

and:

$$r_o = r(x_o, 0) \tag{15}$$

With x_o being the coordinate at which $|r(x, 0)|$ is maximum. Further, the reference refractive indices in Eq. (10) are: $n_0^+ \equiv n(x_0, 0^+)$ and $n_0^- \equiv n(x_0, 0^-)$. Obviously, the refractive index distribution $n(x, 0^-)$ is the refractive index profile of the dielectric waveguide and similarly $n(x,0^+)$ is that one of the plasmonic waveguide $n_p(x)$. The reflection formalism in Eq. (8), has been verified extensively in many situations involving strong reflections, like the laser facet reflectivity [26,36].

The transmitted field $H_t(x,0)$ at z = 0, follows directly from the boundary condition:

$$H_t(x, 0) = H_i(x, 0) + H_r(x, 0) \tag{16}$$

This field will excite all the modes, discrete and continuous [19], of the MIM waveguide in z > 0. After few nanometers, the fundamental TM_0 dominates. As a preliminary test of the method, we considered the following parameters for the waveguides: W_p = 43 nm, W_d = 300 nm, n_d = 3.477, n_m = 0.397-j11.9856 at λ_o = 1.55 μm. These values correspond to optimal transmission between the two guides (as will be seen later). Fig. 4 depicts the evolution of the magnitude of the magnetic field along the

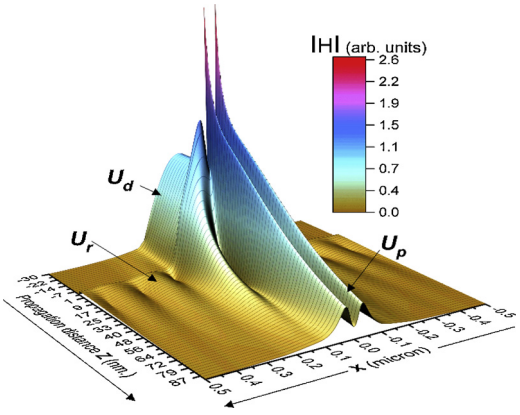

Fig. 4. The TM_0 mode of the dielectric waveguide U_d starts propagation at z = -30 nm toward the MIM waveguide at z = 0. The transmitted field excites strong radiation field U_r at the immediate vicinity of the junction plane. This field fad out, and ultimately, only the fundamental guided plasmonic mode U_p dominates.

propagation direction (dielectric guide length = 30 nm, and plasmonic guide length = 90 nm).

The color contour plot corresponding to Fig. 4 is shown in Fig. 5 which exhibits the main characteristics of the problem: the radiation field generated at z = 0 spreads outside the boundaries of the plasmonic core W_p, and gradually fades out. Finally, the fundamental TM_0 mode of the plasmonic guide predominates.

Fig. 6 is a flow chart depicting the main structure of our computational framework.

It should be emphasized that n_0^+ and n_0^- must not be confused with the index of the homogenous medium used in the BPM algorithm. For z < 0, the reference homogeneous medium assumes the value $n_{od} = \beta_d/k_0$ where β_d is the propagation constant of the TM_0 mode of the dielectric waveguide. Similarly, $n_{op} = \mathrm{Re}(\beta_p/k_0)$ is the reference index of the homogenous medium used in the BPM for z > 0, with β_p being the complex propagation constant of the fundamental TM_0 mode of the MIM guide. These propagation constants are easily calculated numerically [29–30]. The guided transmitted power P_g, few nanometers after z = 0, can be readily calculated as [17]:

$$P_g = \frac{k_0 n_{op}}{2\omega\varepsilon_0}\Re e\left(\int_{-\infty}^{\infty}\frac{|H_t(x, z_0)|^2}{n_{pa}^2(x)}dx\right) \tag{17}$$

where, $n_{pa}(x)$ is the smoothed approximate refractive index profile of the plasmonic guide, and ´ $\Re e$ ' denotes the "real part of". The distance z_o at which the TM_0 mode attains its stable state is estimated by calculating the integral in Eq. (17) at each propagation step for z > 0 until:

$$\frac{1}{2\Delta z}\ln\left[\frac{P_g(z+\Delta z)}{P_g(z)}\right] = const. \tag{18}$$

The criterion Eq. (18) follows directly from the decay rate of the power guided by the TM_0 plasmonic mode [30]. Hence, the power transmission efficiency η is readily calculated:

$$\eta = \frac{P_g}{P_i} \tag{19}$$

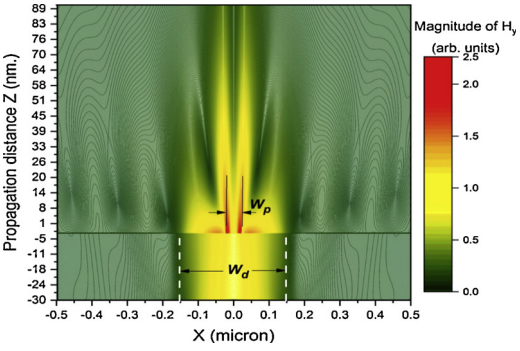

Fig. 5. Contour plot of the total field propagated across the junction plane z = 0. The radiation field excited at junction fades out with distance z and ultimately the TM_0 plasmonic mode predominates.

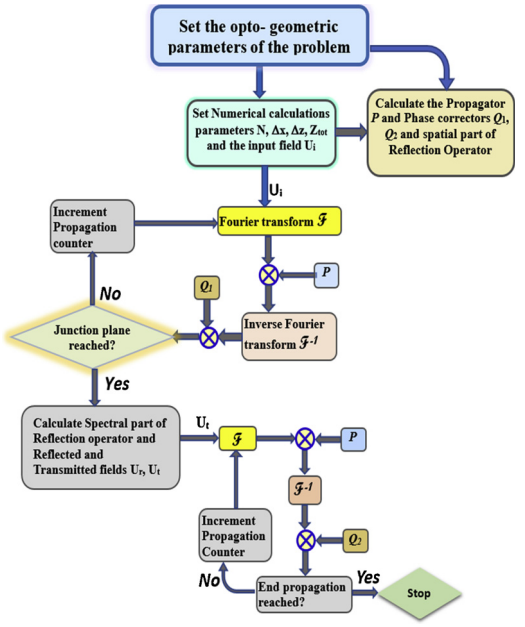

Fig. 6. Flow chart of the implemented program used in the dielectric-plasmonic interconnect.

where, P_i is the incident power at z = 0, namely, the power carried by the guided TM_0 mode in the dielectric waveguide [31]:

$$P_i = \frac{\beta_d}{2\omega\varepsilon_0}\int_{-\infty}^{\infty}\frac{|H_t(x)|^2}{n_d^2(x)}dx \tag{20}$$

where, $n_d\,(x)$ is the refractive index profile of the dielectric waveguide.

Concerning the power stability in the dielectric-plasmonic waveguide coupler of Fig. 3, we checked the intensity I^i of the inhomogeneous part of the total propagated field. The evanescent waves in the angular spectrum of the total propagated field constitute this inhomogeneous field [32]. These waves may degrade the stability of the calculations if they are not well handled. The inhomogeneous intensity I^i (representing the evanescent waves) is calculated from the z-component of the Poynting vector (using Parseval's theorem) as follows [32]:

$$I^i = \int_{k_x>k_o n_o} |h(k_x)|^2 e^{-2\Delta z\sqrt{k_x^2-k_o^2 n_o^2}}dk_x \tag{21}$$

However, a more stringent stability criterion for the evanescent waves is obtained by calculating the energy flux (rather than the intensity) of the inhomogeneous part Φ^i as follows [32]:

$$\Phi^i = \int_{k_x>k_o n_o} \sqrt{k_x^2-k_o^2 n_o^2}\cdot|h(k_x)|^2 e^{-2\Delta z\sqrt{k_x^2-k_o^2 n_o^2}}dk_x \tag{22}$$

according to [32], stability is satisfied if:

$$\Phi^i(z) < \Phi^i(0) \tag{23}$$

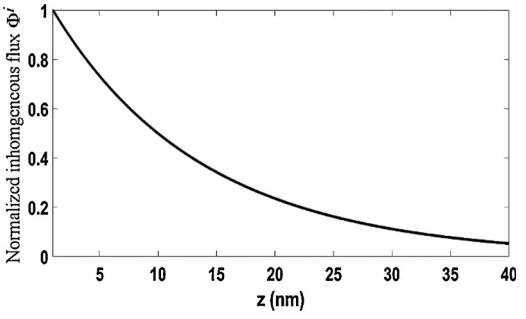

Fig. 7. The energy flux Φ^i of the inhomogeneous component of the total propagated field as function of z. The decay of the evanescent waves constituting that field, reflects the satisfaction of the stability criterion Eq. (23).

we calculated Φ^i as function of z on Fig. 7, which depicts the decrease of the energy flux of the evanescent waves along the propagation direction; hence, the stability of our proposed scheme is satisfied.

It is worthwhile to note that, many researchers have exploited the experimental importance of the plasmonic couplers. Recently [33], it has been reported the experimental realization of a compact, efficient coupler between silicon waveguides and vertical metal-insulator-silicon-metal (MISM) plasmonic waveguides using complementary metal-oxide-silicon technology processes, with copper layers that support low-loss plasmonic modes. Also [34], fabricated an efficient coupler between a dielectric waveguide and a plasmonic metal–insulator–metal (MIM) waveguide using electron-beam lithography and lift-off process. The authors of [35] experimentally demonstrated the nanoscale focusing of surface plasmons by constructing an integrated plasmonic/photonic on chip nano-focusing device in silicon platform. The device was tested directly by measuring the optical intensity along it using a near-field microscope.

4. Numerical results

A FORTRAN program has been implemented to calculate η using the following numerical values:

Number of sampling points along x-axis $N = 2^{16}$, sampling interval along the x-axis $\Delta x = 0.46$ nm, propagation step-size $\Delta z = 0.75\ \Delta x$, propagation distances in the dielectric and plasmonic guides = 20 and 130 nm respectively, hence total propagation distance = 150 nm. The dielectric waveguide core thickness $W_d = 300$ nm, MIM waveguide core thickness W_p varies from 5 to 200 nm, Silicon refractive index $n_s = 3.477$, metal refractive index (silver) $n_m = 0.397$ - j11.4, and the free space wavelength $\lambda_0 = 1.55$ μm. The value of the parameter 'a' in Eq. (7) is set to 20.

At z = 0, we included in the FORTRAN program, the formalism in Eq. (8) to calculate the reflected field, so, the transmitted field $H_t(x,0)$ follows directly from Eq. (16), and propagated by the BPM algorithm in the plasmonic guide. The transmitted power is calculated at each propagation step until the criterion in Eq. (18) is satisfied; and hence η in Eq. (19) is readily obtained. Fig. 7 compares our results with those calculated by the finite difference frequency domain (FDFD) [20].

The maximum efficiency η_{max} occurs at $W_p \cong 42$ nm. Its value is 67.9 % in good agreement with 67.5 % of [20]. The decrease in the transmission efficiency as W_p is increased beyond 42 nm is due to the light confinement characteristics of subwavelength MIM waveguide: at long wavelengths ($\lambda_0 = 1.55$ μm), the field extends relatively in the metal away from the insulator region (air); which means that the effective light-collection cross section is much higher than the geometrical dimension of the insulating layer. That is, the field penetration distance in the metal, around the air core, is much larger than the core width (50 nm) as pointed out in [20]. This is illustrated in our calculations in Fig. 9, which shows the contour plot of the TM_0 mode of the dielectric guide propagated from z = -20 nm towards the MIM guide at z = 0. The guides have $W_d = 300$ nm, and $W_p = 50$ nm. As W_p is increased beyond 50 nm, the effective light-collection area becomes larger than the geometrical dimension of the dielectric guide ($W_d = 300$ nm), thus, the transmission efficiency decreases as illustrated in Fig. 8.

Concerning the complexity and the computational cost of the FFT-BPM; and according to [36,37], with N samples in the transversal direction x-axis and L steps in in the propagation direction z-axis, the required number of multiplications M and additions A to compute an N-point FFT, N-point inverse FFT, are [36]:

$$M = (LN)\log_2 NL + (2LN) \tag{24}$$

$$A = 2LN\log_2 N \tag{25}$$

Conventionally, one complex multiplication needs four real multiplications and two real additions, whereas, one complex addition needs two real additions. Therefore, the number of required real operations takes the following forms [36]:

$$M = (4L.N)\log_2 N + (8L.N) \tag{26}$$

$$A = 6L.N\log_2 N + 4L.N \tag{27}$$

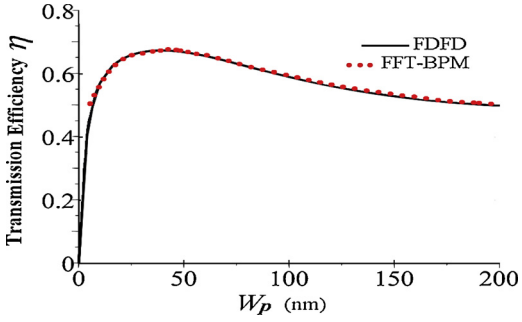

Fig. 8. The transmission efficiency calculated by the Bi-directional FFT-BPM (black continuous curve) and by the FDFD of reference [20]. As W_p increases beyond the maximum point ($W_p = 40$ nm), the light-collection cross sectional area of the MIM guide becomes larger than the core width of the dielectric guide; which in turns, reduces the transmission efficiency.

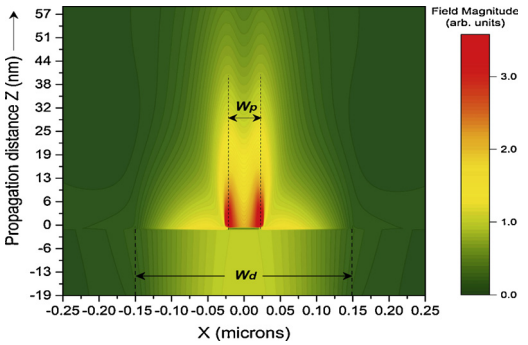

Fig. 9. Color contour plot for the TM_0 mode incident from the dielectric to MIM waveguide at z = 0. The TM_0 mode of the MIM guide dominated the transmitted field few nanometers after the incidence plane. Light power is strongly confined in the core of the MIM guide and field penetrates in the metal around the air gap W_p in the vicinity of the incidence plane.

From the above equations, the time complexity of the FFT-BPM depends on quadratic-logarithmic, i.e. O(LN log2N). Therefore, the complexity (C) for the BPM [38,39] can be expressed as: C = 2 N (4 N + 3), where C is the complexity of one propagation step and N sampling points in the x-direction. However the complexity for L number of propagation steps in the z-direction is equal to (2 N (4 N + 3))L. Thus, the complexity of the FFT-BPM is simpler than the higher-order wide-angle split-step spectral technique [38]. As a practical example, in the coupler problem addressed in sections III and IV, using the following values: N = 65536, total propagation distance Z_{tot} = 200 nm, Δx = 0.465 nm, Δz = 0.348 nm, total number of propagation steps = 574, on a computer with an Intel Core i7- @ 2 GHz, and 16 GB Ram., the calculations are done in 205 s.

5. Conclusions

In this paper, we present remedies to the major difficulties facing the applicability of the FFT-based BPM when investigating TM fields propagation in subwavelength optical interconnects. An equivalent index transforms the TM problem to a TE one, and the step-like index profile of the plasmonic and dielectric guides are smoothed via a smooth transition autoregressive (STAR) function. This enables full exploitation of the advantages associated with FFT-based BPM. A combined spatial-spectral formalism is included in the FFT-BPM formalism to calculate accurately the reflected field at the junction plane between butt-coupled dielectric-plasmonic waveguides. The coupling efficiency exhibits a peak at a certain plasmonic waveguide core width corresponding to matched spot size of both waveguides. We claim that, the method presented in this paper can be extended to other types of very interesting problems, like the evanescent coupling between MIM-dielectric and MIM-MIM waveguides. Such coupling could be very useful and efficient for nanoscale wavelength optical interconnects, sensing, ultra-fast optical switching, and processing.

Author contributions

A.S. and L.R.G. performed calculations and writing. Y.-C. D. Review and Editing. All authors read and approved the final manuscript.

Funding

This study was partially funded by the Allied Advanced Intelligent Biomedical Research Center (A2IBRC) under the Higher Education Sprout Project of Ministry of Education.

Declaration of Competing Interest

None.

Acknowledgments

The authors would like to thank the support from the National Center for Radiation Research (NCRRT) at Atomic Energy Authority in Egypt.

References

[1] M. Ferrera, Y. Park, L. Razzari, B.E. Little, S.T. Chu, On-chip CMOS-compatible all-optical integrator, Nat. Commun. (2010) 1–29.
[2] N. Kinsey, M. Ferrera, G.V. Naik, V.E. Babicheva, V. Shalaev, A. Boltasseva, Experimental demonstration of titanium nitride plasmonic interconnects, Opt. Express 22 (10) (2014) 12238–12247.
[3] N. Kinsey, M. Ferrera, V.M. Shalaev, A. Boltasseva, Examining nanophotonics for integrated hybrid systems: a review of plasmonic interconnects and modulators

using traditional and alternative materials, JOSA B 32 (1) (2015) 121–142.
[4] E.P. Li, H.S. Chu, Plasmonic Nanoelectronics and Sensing, Cambridge university press, 2014.
[5] V.E. Babicheva, A. Boltasseva, A.V. Lavrinenko, Transparent conducting oxides for electro-optical plasmonic modulators, Nanophotonics 4 (1) (2015) 165–185.
[6] L. Chen, J. Shakya, M. Lipson, Subwavelength confinement in an integrated metal slot waveguide on silicon, Opt. Lett. 31 (14) (2006) 2133–2135.
[7] L. Tang, S.E. Kocabas, S. Latif, A.K. Okyay, D.S. Ly-Gagnon, K.C. Saraswat, D.A. Miller, Nanometre-scale germanium photodetector enhanced by a near-infrared dipole antenna, Nat. Photonics 2 (4) (2008) 226.
[8] F.J. Garcia-Vidal, Solid-state physics: light at the end of the channel, Nature 440 (7083) (2006) 431.
[9] H. Raether, Surface Plasmons on Smooth and Rough Surfaces and on Gratings, Springer-Verlag Berlin An, 2013.
[10] S. Nie, S.R. Emory, Probing single molecules and single nanoparticles by surface-enhanced Raman scattering, Science 275 (5303) (1997) 1102–1106.
[11] Y. Inouye, S. Kawata, Near-field scanning optical microscope with a metallic probe tip, Opt. Lett. 19 (3) (1994) 159–161.
[12] W.C. Liu, C.Y. Wen, K.H. Chen, W.C. Lin, D.P. Tsai, Near-field images of the AgO x-type super-resolution near-field structure, Appl. Phys. Lett. 78 (6) (2001) 685–687.
[13] R. Zia, M.D. Selker, P.B. Catrysse, M.L. Brongersma, Geometries and materials for subwavelength surface plasmon modes, JOSA A 21 (12) (2004) 2442–2446.
[14] A. Fadil, D. Iida, Y. Chen, J. Ma, Y. Ou, P.M. Petersen, H. Ou, Surface plasmon coupling dynamics in InGaN/GaN quantum-well structures and radiative efficiency improvement, Sci. Rep. 4 (2014) 6392.
[15] G.F. Dabos, A. Manolis, S. Papaioannou, D. Tsiokos, L. Markey, J.C. Weeber, N. Pleros, CMOS plasmonics in WDM data transmission: 200 Gb/s (8 × 25Gb/s) transmission over aluminum plasmonic waveguide, Opt. Express 26 (10) (2018) 12469–12478.
[16] C. Vassallo, Difficulty with vectorial BPM, Electron. Lett. 33 (1) (1997) 61–62.
[17] L. Poladian, F. Ladouceur, Unification of TE and TM beam propagation algorithms, IEEE Photonics Technol. Lett. 10 (1) (1998) 105–107.
[18] J.P. Boyd, Chebyshev and Fourier Spectral Methods, Courier Corporation, 2001.
[19] Ş.E. Kocabaş, G. Veronis, D.A. Miller, S. Fan, Modal analysis and coupling in metal-insulator-metal waveguides, Phys. Rev. B 79 (3) (2009) 35120.
[20] G. Veronis, S. Fan, Theoretical investigation of compact couplers between dielectric slab waveguides and two-dimensional metal-dielectric-metal plasmonic waveguides, Opt. Express 15 (3) (2007) 1211–1221.
[21] W. Huang, C. Xu, S.T. Chu, S.K. Chaudhuri, The finite-difference vector beam propagation method: analysis and assessment, J. Lightwave Technol. 10 (3) (1992) 295–305.
[22] J. Yamauchi, N. Shimada, Y. Nito, H. Nakano, Transverse-magnetic BPM analysis of a step-index slab waveguide expressed by a sigmoid function, IEEE Photonics Technol. Lett. 21 (3) (2009) 149–151.
[23] H.J.W.M. Hoekstra, P.V. Lambeck, G.J. Krijnen, J. Ctyroky, M. De Minicis, C. Sibilia, O. Conradi, S. Helfert, R. Pregla, A cost 240 benchmark test for beam propagation methods applied to an electrooptical modulator based on surface plasmons, J. Lightwave Technol. 16 (10) (1998) 1921.
[24] L.R. Gomaa, A. Shaaban, M.F.O. Hameed, S.S.A. Obayya, Competitiveness of the BPM in studying the optical beams at critical incidence on dielectric interfaces, Opt. Quantum Electron. 49 (2) (2017) 51.
[25] T. Teräsvirta, Specification, estimation, and evaluation of smooth transition autoregressive models, J. Am. Stat. Assoc. 89 (425) (1994) 208–218.
[26] G. Franssens, P. Kaczmarski, R. Baets, P.E. Lagasse, Extension of bidirectional beam propagation method to TM polarisation and application to laser facet reflectivity, Electron. Lett. 25 (11) (1989) 716–717.
[27] J.W. Goodman, Introduction to Fourier Optics, Roberts and Company Publishers, 2005.
[28] M. Born, E. Wolf, Principles of Optics: Electromagnetic Theory of Propagation, Interference and Diffraction of Light, Elsevier, 2013.
[29] A.R. Zakharian, J.V. Moloney, M. Mansuripur, Surface plasmon polaritons on metallic surfaces, Opti. Express 15 (1) (2006) 183.
[30] S.J. Orfanidis, Electromagnetic Waves and Antennas, Rutgers University, Piscataway, NJ, USA, 2008.
[31] H.F. Taylor, A. Yariv, Guided wave optics, Proc. IEEE 62 (8) (1974) 1044–1060.
[32] M.W. Kowarz, Homogeneous and evanescent contributions in scalar near-field diffraction, Appl. Opt. 34 (June (17)) (1995) 3055–3063.
[33] A. Emboras, R.M. Briggs, A. Najar, S. Nambiar, C. Delacour, Ph. Grosse, E. Augendre, J.M. Fedeli, B. de Salvo, H.A. Atwater, R. Espiau de Lamaestre, Efcient coupler between silicon photonic and metal-insulator-silicon-metal plasmonic waveguides, Appl. Phys. Lett. 101 (2012) 251117.
[34] Ruoxi Yang, Rami A. Wahsheh, Zhaolin Lu, Mustafa A.G. Abushagur, Efficient light coupling between dielectric slot waveguide and plasmonic slot waveguide, Opt. Lett. 35 (5) (2010) 1.
[35] B. Desiatov, I. Goykhman, U. Levy, Plasmonic nanofocusing of light in an integrated silicon photonics platform, Opt. Express 19 (14) (2011) 4.
[36] KamisettyRamamohan Rao, NyeonKim Do, JaeJeong Hwang, Fast Fourier Transform-Algorithms and Applications, Springer Science & Business Media, 2011.
[37] Rohit Chandra, Parallel Programming in OpenMP, Morgan kaufmann, 2001.
[38] A. Shaaban, M. Sayed, MohamedFarhatO. Hameed, Hassan I. Saleha, L.R. Gomaa, Yi-Chun Du, S.S.A. Obayya, Fast parallel beam propagation method based on multi-core and many-core architectures, Opt. Int. J. Light Electron. Opt. 180 (2019) 484–491.
[39] A. Shaaban, Y.C. Du, L.R. Gomaa, Extension of an FFT-based beam propagation method to plasmonic and dielectric waveguide discontinuities and junctions, Appl. Sci. 9 (20) (2019) 4362.